



UNIVERSITY OF
GEORGIA

Department of Statistics

Viability of Structure from Motion to Investigate Historical Rice Growth

Sponsor:
Prof. Marguerite Madden

Authors:
Hayden Crawford
Bryce Davis
Shihan Lyu

19 April 2021

Contents

1	Introduction	1
2	Data Explanation	2
2.1	Wormsloe Site	2
2.2	TLS	2
2.3	UAS	3
2.4	Airborne LiDAR	4
2.5	Digital Surface Models	4
2.6	Digital Terrain Models	4
2.7	Rasters and Rasterization	5
3	EDA	5
3.1	Pasqua's Results	5
3.2	DEM Generation and Comparison	6
3.3	LiDAR Removal and Tide Justification	8
3.3.1	Airborne LiDAR and TLS	8
3.3.2	Low Tide and High Tide DEMs	9
3.4	Discussion of Ergodicity	10
4	Methods: Characterizing the Bias	11
4.1	Between Area Differences	11
4.2	Direct Sunlight vs. Shade	13
4.3	Land and Water	16
4.4	Within Area Differences	18
4.4.1	Vegetation	18
5	Conclusions and Recommendations	20
6	Comparison Tables	22

List of Figures

1	Location of Wormsloe Site	1
2	Wormsloe at High and Low Tide	2
3	The TLS laser scanner (left) and UAS quadcopter drone (right)	3
4	Visual representation of TLS point cloud	3
5	Ground control target as seen from drone footage	4
6	Comparison of DSM and DTM	5
7	Comparison of Binning Methods	5
8	A marsh profile plot from Pasqua's dissertation	6
9	Low tide DEM based on using a TIN (left) and its 3d counterpart (right).	7
10	The maximum binning DEM before and after being overlaid with shapes	7
11	Comparison of LiDAR DEM heights in clearing (top left) and TLS heights (top right) along with the low tide drone heights (bottom) . .	9
12	Georeferenced image (left) vs classified maximum DEM (right) . . .	11
13	Heatmap of Drone Error.	12
14	The variogram comparing variance between cell values as a function of distance over the clearing.	14
15	Kriging over the regions in direct sunlight (left) and shade (right) to generate a map of average bias based on location.	14
16	Differences between our Kriged predictions for error and the actual values for error between the drone and TLS scanner's readings for height for both the areas in sunlight (left) and shade (right)	15
17	The new distribution of cells around their local bias with included variance figures for sunlit areas (left) and areas in shade (right) . .	15
18	Variogram comparing variance between cell values as a function of distance over the clearing and water-covered areas	16
19	Kriging over the regions over land (left) and submerged areas (right) to generate a map of average bias based on location.	17
20	Differences between our Kriged predictions for error and the actual values for error between the drone and TLS scanner's readings for height for both the areas above (left) and below(right) water	17
21	The new distribution of cells around their local bias with included variance figures for areas on land (left) and below water(right)	17
22	Pasqua's ground classified DEM (left) and the maximum binned TLS DSM (right). Around the clearing outlined in purple	19
23	A comparison of the TLS-UAS differences across the clearing (left) and the TLS DEM-DSM differences across the clearing (right). The DSM has some holes where extreme values were removed.	19
24	Scatterplot of the differences in TLS and UAS values with the difference in the TLS DEM and DSM	20

List of Tables

1	Directly comparing low and high tide “error” against the TLS results	10
2	Comparison of Moran’s I measure for autocorrelation before and after fixing error around local bias	14
3	Comparison of Moran’s I measure for autocorrelation before and after fixing error around local bias	17
4	A comparison of all low tide DEM generation method to their TLS counterpart	22
5	A comparison of all low tide DEM generation method to their LiDAR counterpart	22

1 Introduction

Located in Savannah, Georgia, Wormsloe is a state historic site that represents one of the most significant historical, cultural, and natural sites in the southeastern United States (Figure 1). Due to its heritage of land stewardship, archaeological findings, colonial settlement, plantation agriculture, post-Civil War subsistence farming, and depression era tourism, Wormsloe occupies a mainspring of the antebellum South. Though limited access to freshwater and absence of direct evidence typically obviates Wormsloe as a rice cultivation site, an 1880 agricultural census mentioning the cultivation of 510 pounds of rice and an enclosed upland rice sample from a 1772 exchange between Benjamin Franklin and Wormsloe founder Noble Wimberly Jones contests this notion (Swanson, 2012). In an unpublished dissertation, Dr. Alessandro Pasqua investigates the possibility of rice cultivation at Wormsloe. From the abstract, Pasqua (2015) explains,

“The primary goal of this study, therefore, is the investigation of clues within the Isle of Hope landscape [Wormsloe] that may provide legacy evidence of rice cultivation and place Wormsloe within the agricultural context of the Southeastern U.S. coast in the 18th and 19th centuries. Through advanced remote sensing techniques such as terrestrial laser scanning (TLS) and uncrewed aerial systems (UAS) ... to provide archaeological evidence of historical rice cultivation.”

The advisory committee that reviewed Pasqua’s dissertation rejected its publication due to inadequate analysis of the aforementioned remote sensing techniques. Our study aims to perform such analysis missing from Pasqua’s submission and derives its findings from the same data used in Pasqua’s dissertation. The existence of rice cultivation or lack thereof is not of importance in this analysis. Rather, we will investigate and characterize the bias of these remote sensing techniques. Specifically, the viability of Structure from Motion (SfM), a method of creating 3-D environments from a series projected 2-D images, will be of focus.



Figure 1: Location of Wormsloe Site

2 Data Explanation

2.1 Wormsloe Site

The Wormsloe site is the designated area within Wormsloe used for Pasqua's experiment. The site is a small, inlet marsh with waist-high grasses that floods during high tide. Figure 2 displays low tide (lower left) and high tide (lower right). The study site is about 50 meters long and 15 meters wide. The inlet connects to the ocean through a raised bed, the lower dike (top right), and floods through to another raised bed, the upper dike (top left). The open region between the dikes is what we refer to as the "clearing". Following designation of the study site (Figure



Figure 2: Wormsloe at High and Low Tide

2), several geospatial techniques were applied to detect, map, and measure topographic features indicative of rice cultivation: terrestrial laser scanning (TLS), airborne light detection and ranging (LiDAR), and Uncrewed Aerial Systems (UAS).

2.2 TLS

Pasqua's TLS methodology utilizes a RIEGL VZ-1000 laser scanner - seen in the left panel of Figure 3. The scanner employs a 20 milliradian laser beam stationed atop a tripod that rotates and scans the area in a 450-meter radius. During low tide, researcher Chester Jackson placed the TLS scanner in the four corners of the



Figure 3: The TLS laser scanner (left) and UAS quadcopter drone (right)

collection site. A composite scan combining all four tripod locations generates a point cloud density of 2230 points per square meter. This point cloud is saved as a .LAS file (.LASER), and can be visualized as in Figure 4. In this analysis, the TLS



Figure 4: Visual representation of TLS point cloud

point cloud data is considered as “truth” due to its proximity to the ground, tight point density, a composite of four individual scans, and because it is less susceptible to inter-scan variance. Additionally, it is important to note that the TLS files used to generate the Pasqua’s high and low tide DEM had already been “ground classified” to remove vegetation.

2.3 UAS

The UAS shown in Figure 4 is a Phantom II quadcopter. It flew over the marsh at 60 and 85 feet above the ground to capture varying levels of detail. Two flights were conducted at both the highest and lowest tides of the month. Nine targets were placed in visible locations with their positions recorded by GPS to sync the flights to the proper coordinate system (Figure 5). After the flight, researchers

examined the frames of the video captured by the drone to pick out frames with > 80 % overlap in image contents to form a 3-dimensional representation of the site through a process called structure from motion (SfM). The high and low tide models were constructed in Agisoft Metashaper with 534 and 180 pictures, respectively.



Figure 5: Ground control target as seen from drone footage

2.4 Airborne LiDAR

The study also includes data from an airborne LiDAR flight conducted over Chatham County. Various U.S. departments organized the aerial scan in 2009 and conducted it at 1100 meters above ground level with a 30° field of view camera. The point cloud contains 5.394 points per square meter. This method also saves a point cloud in .LAS, just with far less density than in Figure 4. This only contains ground elevation points.

2.5 Digital Surface Models

The Digital Surface Model (DSM) is a projection of the surface that contains information about above ground obstructions (vegetation, man-made structures, etc.). The red line in Figure 6 represents a DSM. A DSM is constructed by tessellating the points of the .LAS point clouds into a geometric surface in software such as ArcGIS .LAS toolbox or QT Modeler.

2.6 Digital Terrain Models

The Digital Terrain Model (DTM), also known as a Digital Elevation Model (DEM), contains information representing the ground surface of the earth without surface obstructions. This is demonstrated as the cyan line in Figure 6. It is

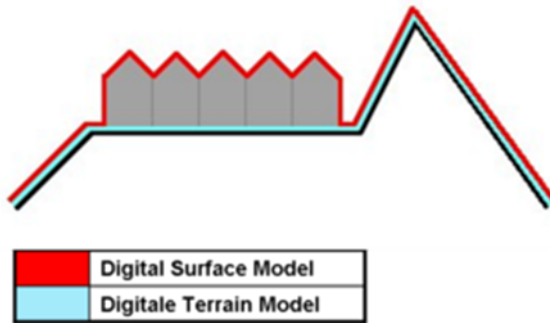


Figure 6: Comparison of DSM and DTM

created in the same way as a DSM, but the .LAS is filtered to only contain ground points before generating a surface.

2.7 Rasters and Rasterization

In this analysis, a raster file corresponds to our DSM or DEM model. A Raster is a grid (x, y, z) of “pixels” or cells that each contain a single height (z), forming a projection, or rasterization of a single surface. We project the height (z) values through a process called “binning”. Binning combines detailed point cloud data into “bins” then assumes a height value based on a function of all points in the bin – lowering its “resolution”. The minimum binning corresponds to the assumed ground classification (DEM) and the maximum binning corresponds to the height of whatever was the tallest in the bin (DSM). Examples of maximum (right), average (middle), and minimum (left) binning can be seen below in Figure 7. Notice the large reduction of vegetation interference in the minimum binning.

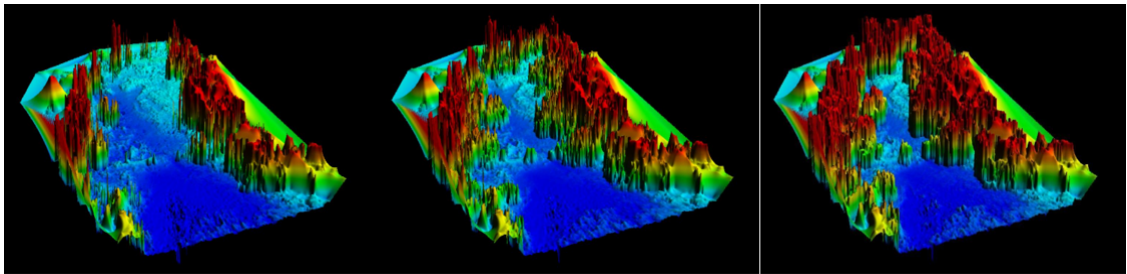


Figure 7: Comparison of Binning Methods

3 EDA

3.1 Pasqua’s Results

There were several problems Pasqua’s data that needed to be addressed. To visualize this, we will use a profile plot that models the height of a surface across

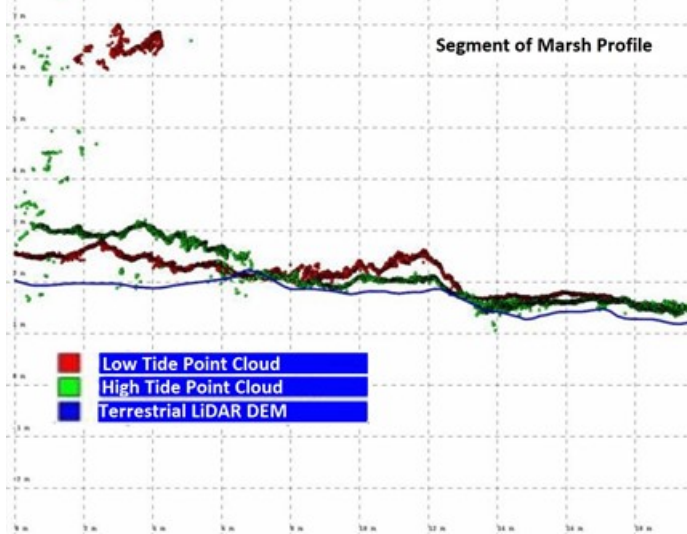


Figure 8: A marsh profile plot from Pasqua’s dissertation

certain distances. For example, Figure 8 above profiles each method’s estimated surface height across the marsh. Pasqua’s results show a large difference (approaching one meter) between the different methods. This large, unexplained difference is a main reason behind the paper’s rejection. Additionally, you may note that two of the lines in Figure 8 are not even surfaces, but instead a tight collection of the point cloud data with visible disturbances along the y-axis. We were also not given a DEM for the drone data. Therefore, in order to perform a proper analysis, we must convert all the data to a single, comparable format. The provided TLS DEMs have the same size of 0.2m x 0.2m for each cell, so this was used as are reference. When generating each drone DEM, we use the resolution of our LiDAR and TLS DEMs (623x370 raster files).

3.2 DEM Generation and Comparison

The first approach we took to making the drone DEMs was using binning. The functions we tested were taking the average, maximum, and minimum of the cells. This is seen above in the panels Figure 7 respectively. We expect that the minimum will estimate the DEM the best, since if vegetation and a ground point share the same cell, the vegetation will be effectively ignored to match a DEM rather than a DSM.

Another way of generating a drone DEM is through a triangulated irregular network (TIN) mesh. This is an alternative to binning to create a single height value for a given resolution of cell. This is seen in Figure 9. One drawback of the drone data is that it is difficult to sort ground points from vegetation due to its lack of a laser scanner. Without this method of filtering, we cannot get our TIN file to take minimums, and it will instead build around averages. The TIN mesh

will produce very similar results to binning on averages seen in the middle panel of figure 7. Overall, the DEMs appear like images we have from the Wormsloe site.

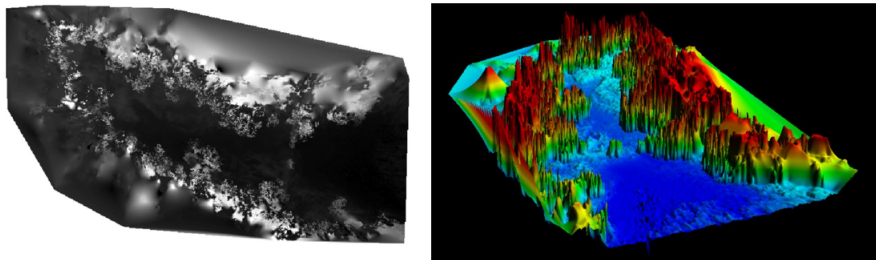


Figure 9: Low tide DEM based on using a TIN (left) and its 3d counterpart (right).

Since Pasqua claims to have constructed TLS and LiDAR DEMs himself, we expect that the minimum binning method will be the best since it is the only one that actively strips away vegetation. While the more heavily forested areas around the edges of the minimum binning DEM still show trees, the method has seemingly managed to knock off almost all of the vegetation above the rice clearing.

Now, we need a way to compare these DEMs to their LiDAR and TLS counterparts along specific regions. Figure 10 shows how we used ArcGIS to make shapefiles based on feature locations. The maximum binning DEM was used in this process as it gave us a clear image of where trees are. From here, we used the

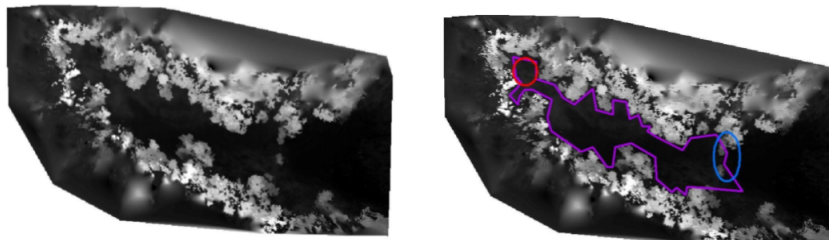


Figure 10: The maximum binning DEM before and after being overlaid with shapes

shapes as masks in RStudio to get some basic information regarding our DEMs and how they compare to the TLS and LiDAR DEMs. For each of the methods described to generate DEMs, we examined the means and variances of the height differences for TLS at Table 4 in the Appendix and airborne LiDAR in Table 5 in the Appendix of all three regions. The information we gain from this is our first real quantification of how the drone's SfM methods can vary from the TLS and airborne LiDAR methods, and it raises some important questions regarding how the data was collected.

Each value for mean difference and variance of error is calculated by converting the

respective DEMs to matrices and taking the difference between heights for each cell, where the mean and variance is then calculated. The bias represents these average differences between TLS or LiDAR and UAS while variance gauges the variance of the difference. As expected, the minimum binning method seems to work the best in producing the least error when comparing against TLS and airborne LiDAR DEMs. However, the mean error for the airborne LiDAR seems to be universally higher (when we say bias, or mean error, is higher, we refer to the magnitude of the number) while at the same time having a much lower variance. One explanation for this phenomenon is that the drone and airborne LiDAR struggle similarly with picking up ground points below vegetation. While we have eliminated the influence of trees by only looking at areas within clearings, there still exists plenty of waist high grass in the swamp that could influence our results. While the airborne LiDAR uses a laser like the TLS, the decreased point density means it is less likely to penetrate the grass. Then, both the drone and airborne LiDAR are similar in their shortcomings. This further suggests that we should use the TLS to correct or model our biases that the vegetation may produce within areas. Another way we aim to examine bias is to model differences between TLS and UAS DEMs between certain areas of interest that may affect drone accuracy such as well and poorly lit areas along with above and below-water regions. After that, we can attempt to examine bias consistency within each region as a result of vegetation.

3.3 LiDAR Removal and Tide Justification

We attempt to identify if the drone can produce more accurate results at high tide or if the airborne LiDAR data is useful. Before attempting to characterize the drone's bias in several areas, we will further investigate these questions to determine if we will use high tide or LiDAR data whatsoever.

3.3.1 Airborne LiDAR and TLS

When drawing bias comparisons between both the airborne LiDAR and TLS versus the different binning methods for the drone data, one easily identifiable trend is how the biases between comparing the drone and the airborne LiDAR are much higher than comparing the drone with the TLS. We know that the TLS yields the "truth" of the surface when compared to the airborne LiDAR, but we did not expect the two laser methods to yield such different results.

Figure 11 shows us just how different the results from these two methods are. The TLS generally presents heights much higher than the LiDAR values. Also, the points are spread out over a much larger range of values outside of what the LiDAR detects. This range of points is also reflected by the drone, whose distribution takes on a mostly similar shape. It is likely that the height of the airborne scanners not only results in a lower point density, but also a loss in the ability to detect slight differences in the heights and properly adapt to elevation changes. While we

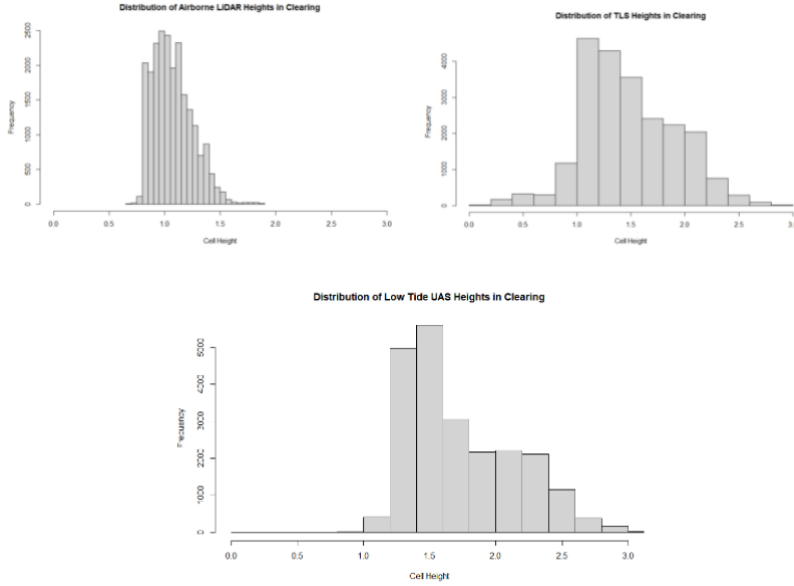


Figure 11: Comparison of LiDAR DEM heights in clearing (top left) and TLS heights (top right) along with the low tide drone heights (bottom)

hoped that the airborne LiDAR might have some place in our analysis on how well the drone might function, the results it yields are so drastically different than the TLS that it would be unreasonable to factor it into further investigation if our goal is to characterize the UAS. The ground-level nature of the TLS that allows it to scan the surrounding areas and get much more accurate results with greater amounts of information makes it the best option for investigating small areas such as the one at Wormsloe, and we will not utilize the LiDAR data in our analysis.

3.3.2 Low Tide and High Tide DEMs

Before now, we have only used our low tide drone data in constructing DEMs. Since the TLS data was also taken at low tide, and water might provide a conflict in how the drone interprets information in relation to the laser methods, we have assumed the low tide was the better option. However, it is still valuable to examine how the high tide drone DEM works in comparison.

We use the minimum binning low tide DEM for the sake of this comparison as it not only best matches the definition of a bare earth DEM but also provided consistently low biases and variances among the areas we examined earlier. Since the high tide point cloud was presented in a different format, we had to create our own high tide DEM in Agisoft Metashaper. The point cloud was first manually edited to remove most overhanging vegetation, then using the auto-classify ground points tool, all but ground points were filtered out. Next, the DEM was generated on the ground points and exported.

	Low Tide (Minimum Binning)	High Tide (Classification and Removal)
Clearing Bias (m):	-0.264	-0.314
Variance (m):	0.116	0.152
Upper Dike Bias (m):	-0.224	-0.048
Variance (m):	0.053	0.149
Lower Dike Bias (m):	-0.694	-0.901
Variance (m):	1.221	0.656

Table 1: Directly comparing low and high tide “error” against the TLS results

Table 1 demonstrates how these high tide and low tide DEMs compare against the TLS. For the most part, the high tide DEM seems to have similarly accurate results to the low tide. In the clearing, the low tide performs better overall but in the upper dike, the low tide has a higher bias but lower variance while it has a higher variance but lower bias in the lower dike. The high tide data is far closer to the low tide data in terms of accuracy than we initially expected. That said, since the TLS scanning was conducted at low tide conditions, we will still favor using the low tide drone data since the high tide drone data, while close, does not offer clear advantages in mapping the surface.

3.4 Discussion of Ergodicity

One of the more important statistical principles relevant to our investigation is the idea of ergodicity. Pasqua only conducted one drone flight over the area and only pieced together one collection of TLS scans at various locations. When we examine comparisons between the TLS and drone methods of mapping the area of investigation, we are breaking the results of these single instances of data collection into groups of cells, which we treat as observations. If, however, this spatial data collection in both the TLS and drone were collected again, it would surely produce different point clouds which, in turn, would produce new DEMs with different values for each cell. How do we quantify this within-cell variance when we only have one value for each cell?

The answer is to assume that the variance we see among different cells of the same DEM around some spatial mean also describes the variance we would see within the same cell across different flights or TLS scans if the process for conducting the scan and drone flight and generating DEMs were the exact same. Then, we can use the information found within one drone flight and set of TLS scans to characterize how future reproductions may differ. This process of quantifying how

a system of randomness can produce different results across several sets of observations by only observing the continual collection of one set of observations is a principle known as ergodicity, and it is crucial in this assessment of drone performance as any information we use could not be otherwise quantified.

Ergodicity is not limitless, and there might be trends among our spatial data that it cannot explain. If we see that the drone's performance is better or worse in some areas in a way that we cannot identify, it may be likely that some factors outside of our knowledge may be randomly producing bias in some areas of the flight.

Ergodicity only explains the variance that each cell experiences independently and cannot be used to quantify characterizations of bias that affects clusters of cells based on their region. If we cannot explain why spatial bias is occurring, we would need to run several drone flights and sets of TLS scans to quantify it across each mapping of the region, which we do not have. With that said, we still will attempt to identify how the drone's performance differs among geographical conditions.

4 Methods: Characterizing the Bias

To begin, we georeferenced a colorized, top-down image of the low tide point cloud in order to classify regions to compare. Figure 12 represents how we used this

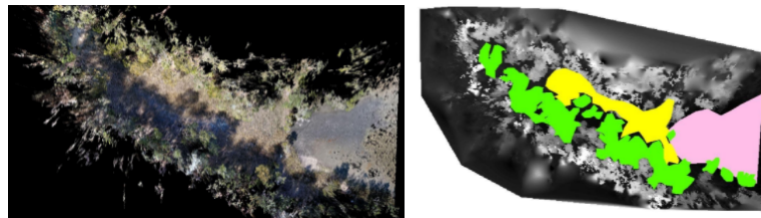


Figure 12: Georeferenced image (left) vs classified maximum DEM (right)

image to characterize the regions. With colors, we can easily identify clearly lit and more shaded areas (in yellow and green, respectively), and the exact location of water (in pink) is easy to identify. We will compare these shaded and bright regions directly with one another and the water to our earlier identified clearing. After that, we will examine how vegetation influences biases within areas.

4.1 Between Area Differences

One of the shortcomings of the drone, as listed in Pasqua's dissertation, is the potential for increased inaccuracy across various types of lighting. Since we can directly identify which areas of the spatial data were in shade and which were in direct sunlight, there is the potential to investigate whether the drone performance was better in areas in direct sunlight. Furthermore, we expect that the drone might interpret water differently than a laser. While most of the study is

conducted above ground, it still might be useful to see if the drone interprets water more poorly than it does land, since some of the area of investigation might be thinly submerged in water.

The first step to our approach should be examining the autocorrelation among our “error”, or TLS-drone difference figures. Spatial autocorrelation refers to the closeness of a response variable based on the closeness of where that response was evaluated. In this case, our response of interest is the error between two spatial data collection methods, but that is calculated as the difference of their heights, which is heavily dependent on location; since these elevations are clearly autocorrelated, we can also expect that the error between the drone and the TLS to be autocorrelated as well. We can get a good idea of how true this is by looking at a “heatmap” of the error. In Figure 13, the x and y coordinates of the graph

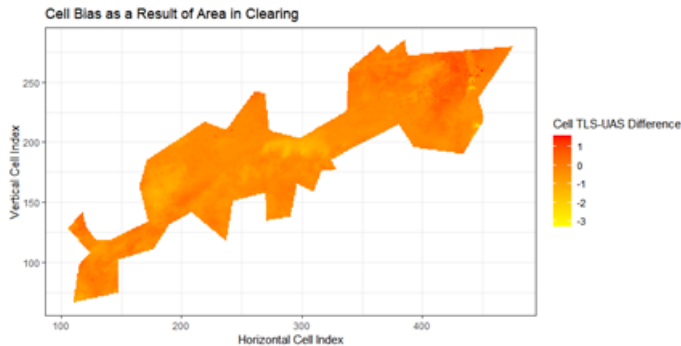


Figure 13: Heatmap of Drone Error.

indicate respective x and y locations, and the color denotes the error of the drone based on the legend off to the right. It is important to note how the errors of the drone appear to be similarly colored “blobs”. If the errors across the plain were not autocorrelated, the colors would look like static, indicating total randomness in location. Instead, areas of higher and lower error are clustered together, suggesting that there is a significant relationship here between the errors of the drone and the cells’ position. This provides a significant limitation in how we can interpret our results. The previously described assumption of ergodicity can explain how the cells can capture the variance in the height values for each cell independently, which does not apply for spatially oriented clusters. Since this bias correlation is based on cell location, and the groups of cells we are comparing are in completely exclusive locations (land vs. water, sunlight vs. shadow), we cannot adequately evaluate bias across these areas in a meaningful way. That said, there is still some investigation open to us. If we characterize the bias across the entire region as a whole and look at drone errors in relation to local bias, we can get an idea of how

precisely the drone performed in these two locations by comparing the variance of adjusted cell errors in these two locations. Since the spatially autocorrelated bias is accounted for and removed in this scenario, this method offers at least some insight into the nature of how this drone may function.

There are several steps we will follow in making these two comparisons for drone consistency. First, we will estimate the autocorrelation across the area by taking a subset of evenly spaced points and viewing that relationship as a variogram, a graph that plots variance as a function of cell distance. Then, we will use this measure to conduct Kriging across our areas of interest. Kriging should generate a map of average height values based on the x and y coordinates of each cell within our regions. Then, we can take the difference between these Kruged predictions for error and our actual differences to get distributions of cell errors adjusted around their local bias. We will examine these distributions to check if we properly eliminated most of the autocorrelation and check for normality. Finally, we hope to compare the variance of these cells to determine if the drone is more precise on land and in the sunlight based on the distribution that the values take. If the distributions of the bias-adjusted cells do not seem to follow any distribution, we will estimate sample variance through bootstrapping.

4.2 Direct Sunlight vs. Shade

In this section, we will investigate the drone's performance in the region we identified to be in shade overcast by trees and the regions in direct sunlight to investigate our theory that the drone precision is greater in areas with more lighting. To begin, we will take one out of every ten cells in the clearing as whole and construct a semi variogram around the information to visualize the autocorrelation we are dealing with. The reason we use 10% of the cells is simply to make the calculations quicker without losing too much information; in this case we have 22,296 cells, which would make Kriging extremely time intensive. The variogram in Figure 14 represents how cells closer together experience less variance between their values than those further apart. The "range" of the variogram is the distance at which the line flattens, and the cells no longer experience the effect of autocorrelation. In this case, the range is 31.794, suggesting that cells have at least some relation to every other height value at a distance of 31 cells away. This high value suggests an extremely strong autocorrelation effect. Two other important aspects of the variogram to consider are the "nugget" and "sill", which represent the y-intercept and asymptotic variance, respectively. By taking the ratio of the nugget to the sill, we can further get an idea of how strong the autocorrelation is; all values lie on a range of 0 to 1, and values closer to 0 are highly autocorrelated while those closer to one are not. In this case, the nugget is 0.010 and the sill is 0.092, putting the ratio at 0.107. This ratio is close to 0, further demonstrating the incredibly significant effect of autocorrelation on TLS-UAS cell differences.

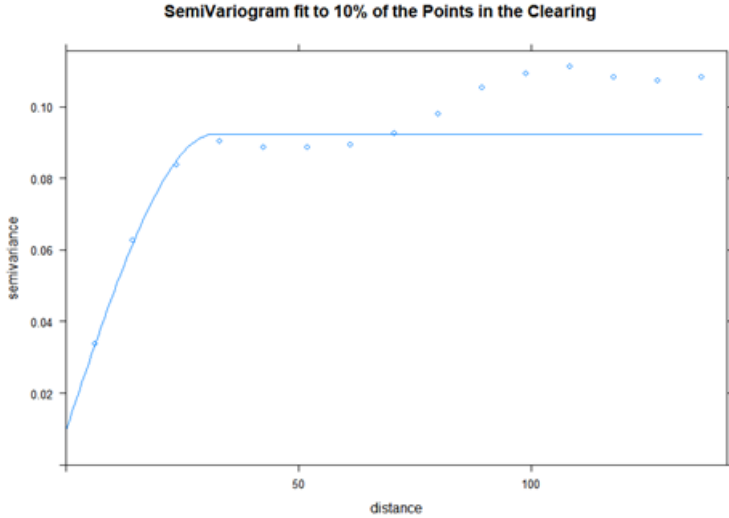


Figure 14: The variogram comparing variance between cell values as a function of distance over the clearing.

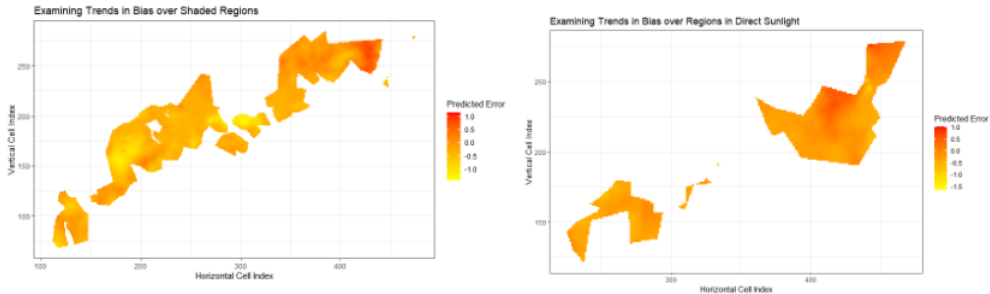


Figure 15: Kriging over the regions in direct sunlight (left) and shade (right) to generate a map of average bias based on location.

The results of Kriging in Figure 15 capture the trends in bias that we saw in our differences between the TLS and drone data earlier through predicting average values for the error in height based on location information. Our goal, as stated before, is to remove the effect of this bias on the error cells contained within the regions to directly compare their variances. Then, we will take the differences between the average values for their height and the true values for height to investigate drone precision.

Moran's I	Before	After
Sunlight	0.234	0.022
Shade	0.291	0.023

Table 2: Comparison of Moran's I measure for autocorrelation before and after fixing error around local bias

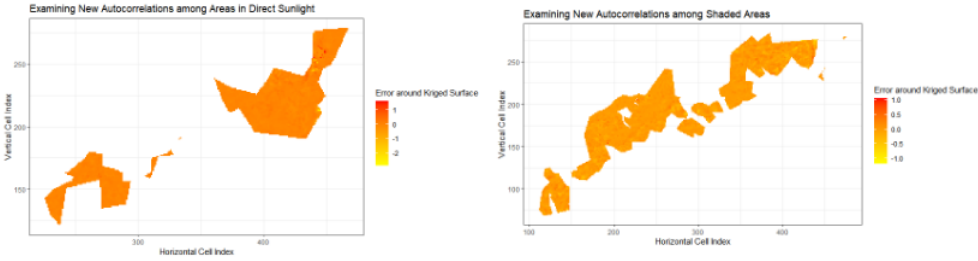


Figure 16: Differences between our Kriged predictions for error and the actual values for error between the drone and TLS scanner's readings for height for both the areas in sunlight (left) and shade (right)

Figure 16 shows our new adjusted differences based on cell location. Of course, they are still not perfectly independent from one another - they are still slightly grouped to a much lesser extent; however, we feel as though we have eliminated enough of the spatially correlated local bias to be able to assess precision. Moran's I is a measure to determine how clustered values are based on the geographic space they occupy. The measure can produce values in the range of -1 to 1, with 1 representing responses totally dependent on autocorrelation. Perfectly scattered values will produce values close to -1, but large distributions of values not at all autocorrelated will tend to produce values close to 0. The Moran's I measure for autocorrelation in Table 2 further demonstrates the drop in spatial dependence. In this case, the values of 0.234 and 0.291 for cells in direct sunlight and shade, respectively, demonstrated high spatial autocorrelation, while the newly produced values for 0.022 and 0.023 demonstrate much less dependence regarding placement. While the values are still positive, suggesting some autocorrelation, we did not expect Kriging to work perfectly and are satisfied with continuing. The final step

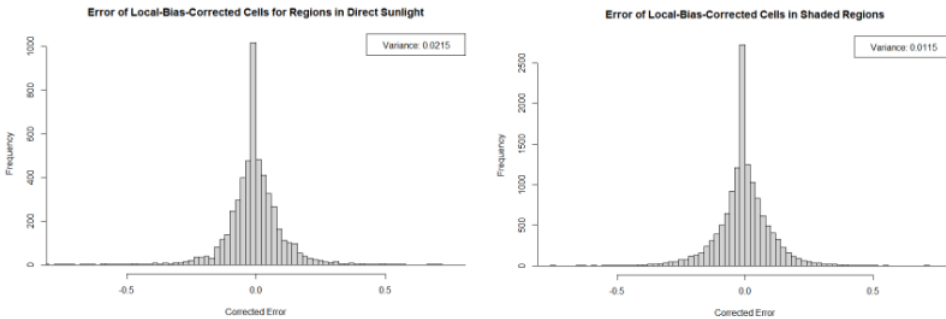


Figure 17: The new distribution of cells around their local bias with included variance figures for sunlit areas (left) and areas in shade (right)

in our analysis is to examine the distributions to identify the best way to quantitatively analyze the variances. Figure 18 above demonstrates that these groups of bias-adjusted cells seem best represented as some Laplace distribution,

meaning that it would be a safe assumption to make in an analysis of their variances. Further analysis, however, is unnecessary, as the variance of the shaded region is much lower; no evidence suggests that the drone yields more precise results in direct sunlight than shade.

4.3 Land and Water

In this section, we will follow the same process to assess drone precision over the areas partially submerged in water versus those entirely on land. Like before, we will start construction of a variogram over both the clearing and the water. Figure

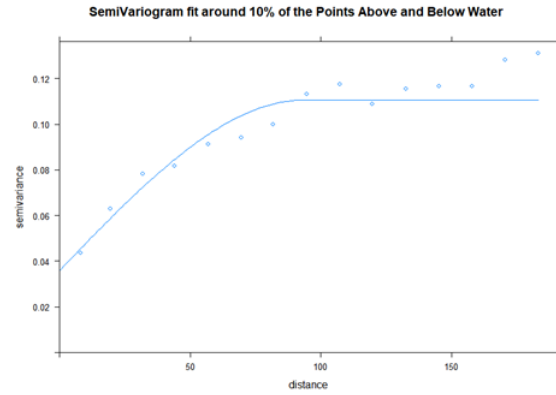


Figure 18: Variogram comparing variance between cell values as a function of distance over the clearing and water-covered areas

18 shows a variogram similar to the one found to compare the areas in sunlight and shade. This variogram, however, includes the areas submerged in water as well, which produces some noticeable changes in its attributes. The range has increased substantially from 31.794 to 93.97, indicating that the cells in the regions covered by water have an autocorrelative effect that persists even further out than those on land. Also, the nugget-sill ratio is much greater in this case, at 0.324 instead of 0.107. While the errors for cell height are still clearly autocorrelated in this case, constructing the variogram has increased the measure significantly. The most likely explanation for this is that the nature of the bias changes in areas that are partially submerged, but as stated before, while we can characterize this bias, it is impossible to explain it in any significant manner with the presence of such high autocorrelation.

Figure 19 demonstrates the results of applying the Kriging over the new surface. Again, we are identifying and quantifying the trends in bias that we see here with the aim of removing them from the error values we have

The results in Figures 20 and 21, as before, do demonstrate that the TLS-UAS error does exhibit some trend in bias even after applying Kriging. The graphs in Figure 20 show that the errors are still clearly clustered together in some points,

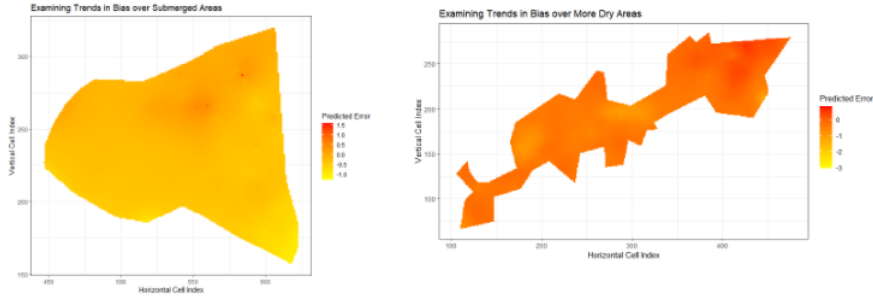


Figure 19: Kriging over the regions over land (left) and submerged areas (right) to generate a map of average bias based on location.

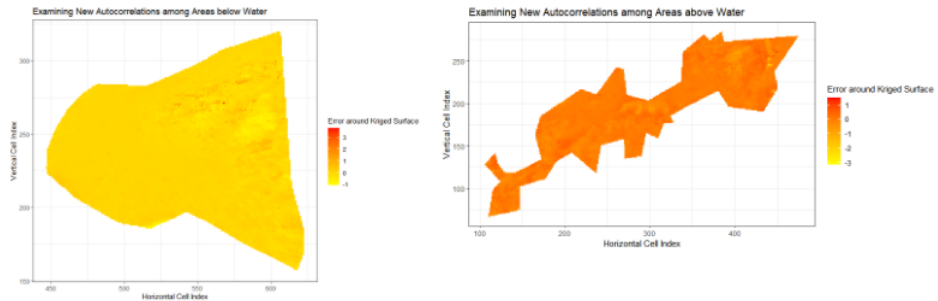


Figure 20: Differences between our Kriged predictions for error and the actual values for error between the drone and TLS scanner's readings for height for both the areas above (left) and below(right) water

Moran's I	Before	After
Land	0.223	0.0478
Water	0.202	0.0368

Table 3: Comparison of Moran's I measure for autocorrelation before and after fixing error around local bias

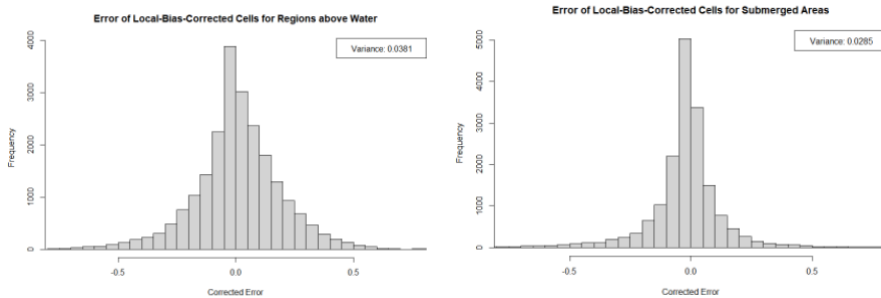


Figure 21: The new distribution of cells around their local bias with included variance figures for areas on land (left) and below water(right)

and Table 3 shows us that some autocorrelation is still left over. Despite this, we still feel as though we have reduced its effect to be able to properly gauge precision.

As before, the corrected error cells in the water and on land seem to follow a Laplace distribution, but the results as far as our theories go are the same; since the variance of the drone's readings is greater on the land than in the water, there is no reason for further analysis. We have no evidence to suggest that the drone gets more precise readings over the land. In fact, the extremely low values we get for the variance might be a good reason to investigate the opposite effect.

4.4 Within Area Differences

The overall trend in spatial bias that we see reflected in Kriging in the previous section is the main problem that contributes to the overall poor results of the drone's mapping of the swamp. From reading Pasqua's dissertation, we can identify two major causes for the error patterns across the UAS flight of the area. The first of these is the set of factors that affect drone flight. High wind, low stability of the drone, and poor or inconsistent angles are all factors that could affect the flight of the drone and produce these clustered errors we are seeing when examining TLS-UAS differences. The other factor is the vegetation in the swamp. It is likely that the drone's SfM process has a limited capacity to properly identify the elevation of the swamp under some of the waist-high vegetation and instead interprets the grass to be land. On the other hand, the TLS scanner's lasers can penetrate much of the vegetation and more properly yield ground level results.

It is unlikely that we could properly formulate a way to explain trends in bias through quantifying factors that could affect the drone's flight. It would be impossible to look each at the frames used in constructing the point cloud, properly quantify how the continual flight video could have produced irregularities in the images, and further translate that result into the context of how certain regions of the DEM are affected.

That said, we still have the means to tackle the vegetation question. When the TLS scanner collects points, it can pick up values at both the top and bottom of the vegetation, so if we use Pasqua's original point cloud that he collected through use of the scanner, we can bin these points on their maximum values and find the difference between this new vegetation-based DEM and his original ground-classified DEM to estimate the quantity of vegetation in each cell. Then, we can compare these cells against the error cells to identify if they are the main source of our trends in bias.

4.4.1 Vegetation

To begin, we will generate a TLS DSM using the original point cloud obtained from the four TLS scans conducted by Pasqua that is based on maximum binning.

This DSM will include vegetation in its elevation estimates, which sets it apart from the TLS DEM that represents bare earth elevation. This DSM in Figure 22

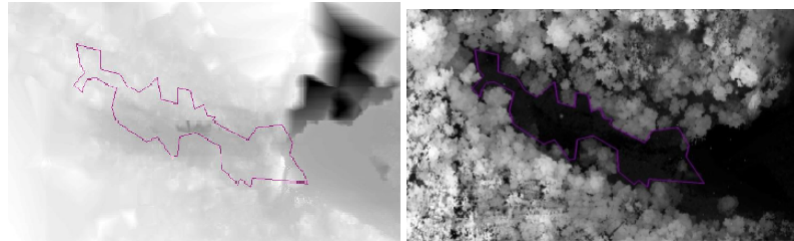


Figure 22: Pasqua's ground classified DEM (left) and the maximum binned TLS DSM (right). Around the clearing outlined in purple

on the right is clearly influenced by vegetation; outside the clearing you can see that it has captured the heights of all the trees in the surrounding areas. Of course, we are only interested in the points within the clearing, and we will find the difference between this DSM and DEM to get an idea of how the vegetation works across this clearing. Figure 23 gives us the first characterization of how

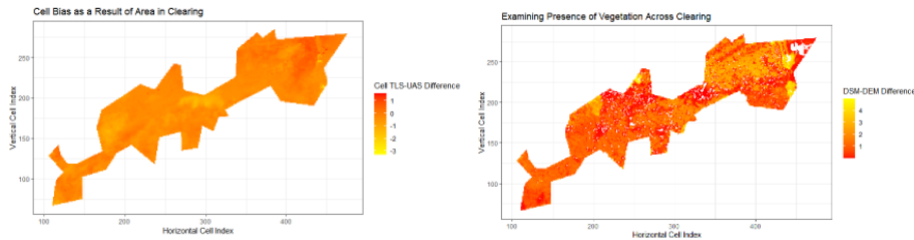


Figure 23: A comparison of the TLS-UAS differences across the clearing (left) and the TLS DEM-DEM differences across the clearing (right). The DSM has some holes where extreme values were removed.

vegetation might affect how our bias is characterized across the flight. On the left is the heatmap used earlier to examine the trends as a whole and on the right is a new heatmap demonstrating the differences in the DSM and DEM. In both cases, if our theory that the bias is a result of increased vegetation is true, the yellow and red areas should, for the most part, match up with one another; more negative TLS-UAS differences indicate higher values of the UAS that could be a product of vegetation, and more positive TLS DSM-DEM differences indicate higher values of the DSM that map vegetation. This, however, does not seem to be the case. Immediately, the patterns in vegetation and bias seem to function completely independently of one another. To better understand and further investigate this correlation, we can use a scatter plot to plot the two types of differences against one another. Figure 24 shows a plot of the two sets of differences against one another, giving us an idea of how the two values might be related for each cell. In

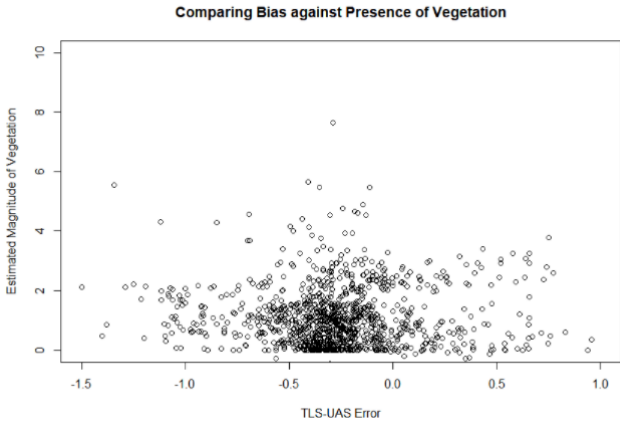


Figure 24: Scatterplot of the differences in TLS and UAS values with the difference in the TLS DEM and DSM

a scenario where the amount of vegetation influenced the bias, the points would be positioned along a downwards trend in which almost no TLS-UAS error would be present when our estimate for vegetation was 0; however, as before, there seems to be no relationship between the two values, and they seem to operate independently of one another. At this point, we can state that it is likely the overall trends in spatial bias across the region are not the product of vegetation, but some other factor. The more likely explanation is that the various factors affecting the pattern of the drone flight such as stability and angle are the reason that such trends in bias exist. Additionally, we can not rule out human error in the manual process of selecting images for the structure from motion technique.

5 Conclusions and Recommendations

Overall, there is a very limited scope to what we may infer with our given information. From examining lighting and water, we find no evidence that shade or water tend to affect drone precision in producing a model of the surface similar to what the TLS identifies; however, we lack the ability to meaningfully quantify and examine bias-affected accuracy when comparing between these areas as its presence is extremely location-dependent, and we only have results from completely separate areas. One solution to getting a better understanding of how lighting may affect the results would be to compare results of a drone flight when the sun is directly overhead against when most of the area is covered in shade so that we could compare our TLS-UAS differences within the results for each cell. As far as a proper water-focused solution might go, one might be able perform a laser scan during high tide, take the difference between that and the already collected high tide drone flight, and compare it against the same respective difference for the low tide scan and drone flight.

Probably the best solution to more intimately understand the nature of the spatially-correlated bias would be to perform a series of several more flights to examine if it would manifest similarly in future constructions of the terrain. If several more flights yielded the same groupings of bias as what we have seen in the past, then we would know that the biases were likely the result of some geographic feature. Already we have examined the possibility of vegetation being the culprit, but we did not find that that was the case. Should the bias manifest differently every time, and factors affecting the flight or method of stitching frames together be the issue, then we would most likely have to understand the process of spatial bias as the product of some random process that we cannot specifically quantify. If this is the case, it might further be a good idea to consider pooling the point clouds of several flights so that the bias may eventually even out and form a DEM far more uniform in bias and compare that to the TLS scanner's results. A controlled experimental design could also be performed controlling for specific conditions that may induce drone inaccuracy.

6 Comparison Tables

	TIN	Average	Maximum	Minimum
Clearing				
Bias (m):	-0.372	-0.371	-0.483	-0.264
Variance (m):	0.155	0.147	0.272	0.116
Upper Dike				
Bias (m):	-0.330	-0.330	-0.432	-0.223
Variance (m):	0.053	0.051	0.062	0.053
Lower Dike				
Bias (m):	-1.169	-1.889	-1.889	-0.694
Variance (m):	2.928	5.964	5.964	1.221

Table 4: A comparison of all low tide DEM generation method to their TLS counterpart

	TIN	Average	Maximum	Minimum
Clearing				
Bias (m):	-0.768	-0.767	-0.879	-0.660
Variance (m):	0.135	0.125	0.248	0.092
Upper Dike				
Bias (m):	-1.301	-1.301	-1.403	-1.195
Variance (m):	0.037	0.035	0.046	0.036
Lower Dike				
Bias (m):	-1.061	-1.080	-1.781	-0.586
Variance (m):	1.851	1.694	4.416	0.575

Table 5: A comparison of all low tide DEM generation method to their LiDAR counterpart